Determination of the magnetic structure of Mn_3Sn using generalized neutron polarization analysis

Determination of the magnetic structure of Mn_3Sn using generalized neutron polarization analysis

P J Brown†, V Nunez†, F Tasset†, J B Forsyth‡ and P Radhakrishna§

† Institut Max von Laue–Paul Langevin, BP 156X, 38042 Grenoble, France
‡ Rutherford Appleton Laboratory, Chilton, Oxon OX11 0QX, UK
§ Laboratoire Leon Brillouin CEN Saclay, 91191 Gif-sur-Yvette, France

Abstract. The newly developed technique of generalized polarization analysis has been used to re-examine the triangular magnetic structure of Mn_3Sn. The magnitude and direction of the polarization of neutrons scattered by some mixed magnetic and nuclear Bragg reflections at 200 K have been measured for a range of different incident polarization directions using a zero-field polarimeter. The results have been used to discriminate between different models which have been proposed for the magnetic structure. The analysis shows unambiguously that a structure allowing three trigonal domains is necessary to account for the scattered polarizations. Of the models suggested up to now only the 'inverse triangle' structure satisfies this criterion. The manganese moment was determined to be 3.00(1) μ_B much larger than the value (1.78 μ_B) given by earlier measurements of the flipping ratios in an applied field. On cooling below 50 K the polarization analysis gave evidence for a transition to a magnetic structure with a significant ferromagnetically aligned moment parallel to [001].

1. Introduction

The complex magnetic behaviour of the isostructural intermetallic compounds with nominal compositions Mn_3Sn, Mn_3Ge and Mn_3Ga has been the subject of a number of studies since the first two of these compounds were shown to exhibit weak ferromagnetism by, respectively, Yasukochi *et al* (1961) and Ohoyama (1961). The basal plane projection of their DO_{19} structure, space group $P6_3/mmc$, is shown in figure 1. The atomic sites are:

Atom	site	site symmetry	coordinates		
Mn	6h	mm	x	$2x$	$1/4$
Metalloid	2c	$6m2$	$1/3$	$2/3$	$1/4$

The structure is generally stable only in the presence of excess Mn: in the Mn–Sn system, Mn atoms replace Sn to stabilize the structure over the range of composition $Mn_{3.2}Sn$–$Mn_{3.7}Sn$. For $Mn_{3.34}Sn$ at room temperature the cell dimensions are $a = 5.665$, $c = 4.531$ Å and the value of the parameter x above is 0.8388(2) (Tomiyoshi 1982).

The first neutron diffraction measurements were made on polycrystalline samples of Mn_3Sn and Mn_3Ge by Kouvel and Kasper (1965) who deduced that their antiferromagnetic structures were based on a triangular arrangement of manganese magnetic moment directions lying in a plane containing [001]. They confirmed that the onset
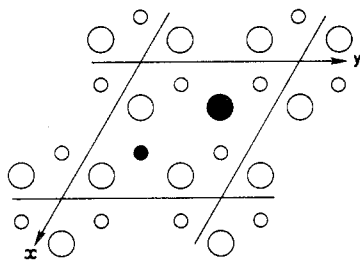
Figure 1. The [001] projection of the DO_{19} structure adopted by Mn_3Sn, Mn_3Ge and Mn_3Ga. Manganese atoms are shown as open circles, the larger being at height 1/4, the smaller at 3/4. The metalloid positions are shown as solid circles, the larger again being at height 1/4 and the smaller at 3/4.

of weak ferromagnetism in $Mn_{3.7}Sn$ at 420 K coincided with the Néel temperature, T_N, and noted that its disappearance at around 220 K was accompanied by a splitting of the (101) magnetic reflection into a pair of satellites associated with a propagation vector parallel to [001] and a period of about 45 Å. This modulation persisted unchanged to 4.2 K but below 50 K they observed an upturn in the magnetization to a value greater than that observed in the temperature interval 270–420 K. Neutron powder diffraction experiments were also performed by Krén and Kádár (1970) on Mn_3Ga, by Kádár and Krén (1971) on Mn_3Ge and by Zimmer and Krén (1973) on Mn_3Sn. The latter authors confirmed the triangular nature of the spin arrangement at room temperature for a sample with 72.0(2) at% Mn ($Mn_{3.34}Sn$), but concluded that the moments of 2.4(2) μ_B lay in the basal plane, as did the small ferromagnetic moment of 0.003 μ_B/Mn. These authors also prepared single crystal samples of the same composition and found that annealing at temperatures between 550 and 800 °C was necessary to produce the long period modification of the magnetic structure first observed by Kouvel and Kasper (1965). Single crystal samples of $Mn_{3.34}Sn$ were also prepared by Tomiyoshi (1982) who determined the polarization dependence of the scattered neutron intensity in $\{h0l\}$ and $\{hhl\}$ reflections with the sample at room temperature and in an 0.8 T field along [010] and [1−10] respectively. These data enabled him to confirm that the spin structure was indeed triangular with the spins in the basal plane but did not allow him to determine whether the spins lie parallel to [100] or [110]. The manganese moment was found to be 1.78(2) μ_B at 293 K which extrapolates to some 2.1 μ_B at 0 K. In a subsequent series of measurements Tomiyoshi and Yamaguchi (1982) claimed to have resolved the structural ambiguity through measurement of the flipping ratios as a function of rotations of the specimen about the scattering vector, again in an external field of 0.8 T. They concluded that the structure corresponds to the 'inverse triangle' model first proposed by Zimmer and Krén (1973).

As a result of the measurements already referred to and additional single crystal studies by Ohmori *et al* (1987) and Tomiyoshi *et al* (1986 and 1987), it is clear that both stoichiometry and thermal treatment influence the magnitude of the weak ferromagnetism which appears below T_N, the temperature T_1 at which this weak ferromagnetism reduces to near zero, the appearance or not of the incommensurate magnetic phase below T_1, the temperature T_2 at which the magnetization again begins to increase and its maximum low temperature value (see figure 2). T_1 has been reported in the range 150–270 K and T_2 in the range 100–50 K. The magnetization below T_2 is greatest along [001] and amounts to some 5.3 emu g^{-1} at 4.2 K; however, Tomiyoshi *et al* (1986) could detect no significant changes in the integrated neutron intensities for a number of low angle magnetic reflections in the temperature range 4.2–100 K.

The object of the present experiment was to see to what extent the use of generalized polarization analysis would enable us to determine the exact nature of the triangular
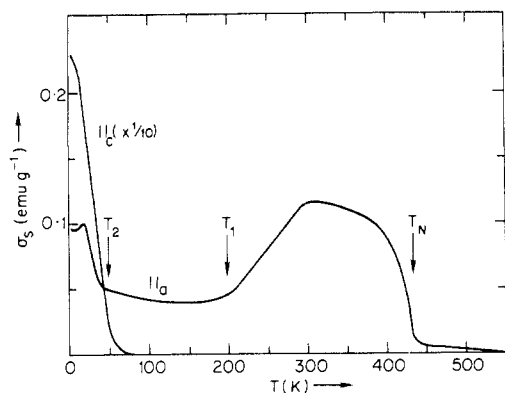
Figure 2. The temperature dependence of the spontaneous magnetization parallel ($\parallel$) and perpendicular ($\perp$) to the c axis of the sample of $Mn_{3.2}Sn$ used in the present experiments (Ohmori 1986).

structure, its domains and the magnitude of the Mn moment. One advantage of the technique is that the specimen is in zero external magnetic field, so its domain structure remains constant throughout the experiment. This is in contrast to the polarized beam experiments of Tomiyoshi (1982) and Tomiyoshi and Yamaguchi (1982) in which the magnetizing field of 0.8 T was known to influence the domain structure, but to an extent which was difficult to determine and which could influence the magnitude of the moment contributing to the observed flipping ratios. We have also made measurements down to 5 K and, for the first time, observed gross effects in the neutron scattering associated with the phase stable below T_2.

2. Models for the magnetic structures of DO_{19} compounds

The magnetic structures that are compatible with the symmetry of the DO_{19} structure and its sub-groups have been discussed by Zimmer and Krén (1973) and by Tomiyoshi (1982). Their results may be summarized as follows. The structures that retain the full symmetry $6_3/mmc$ are (1) the ferromagnetic one with all spins parallel to c, (2) a group of structures in which spins related by the inversion structure are oppositely directed, and (3) the two triangular structures of figure 3(a) and (d). All these structures may be rejected on the basis of experimental evidence, the first from the magnetization the second from the absence of a 111 reflection in the diffraction pattern, and the third from the presence of both 100 and 110 reflections in the patterns. Structures which are compatible with the powder diffraction intensities can be obtained by relaxing the symmetry in either of two ways. One possibility is to remove the mirror symmetry perpendicular to $\langle 100 \rangle$ in the magnetic structures. This allows the spins to have a general orientation in the (001) planes so that both 100 and 110 reflections can occur; their relative intensities depend on the absolute spin orientation. The relative orientations of the spins for two particular cases in which the spins are in $\langle 100 \rangle$ and $\langle 1-10 \rangle$ directions are illustrated in figure 3(b) and 3(e) respectively. Alternatively the hexagonal symmetry axis may be reduced to just a diad. This gives the two structures 3(c) and 3(f), both of which have orthorhombic magnetic symmetry. Other structures with yet lower symmetry are possible. However, both the structures with reduced hexagonal (6/m) symmetry and the orthorhombic 'inverse triangle' structures are able to account for the observed magnetic diffraction, and indeed predict very similar diffraction intensities. Finally only the structures with orthorhombic symmetry, which allow inequivalence between the manganese atoms, are compatible with the weak ferromagnetism which is observed in the (001) plane.
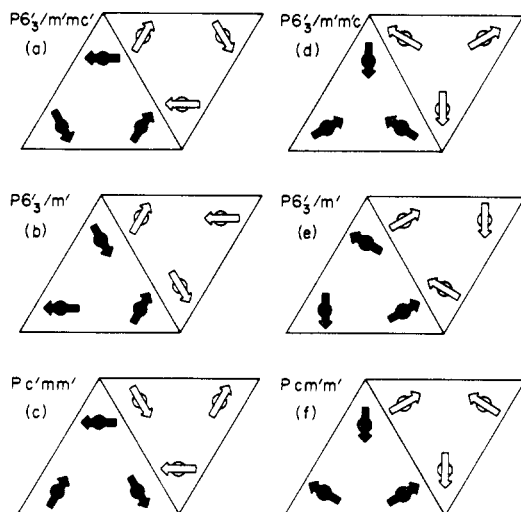
Figure 3. Some of the possible spin configurations allowed by the full symmetry of the DO$_{19}$ structure ($P6_3/mmc$) and its subgroups. In (a), (b) and (c) the spins are parallel to $\langle 100 \rangle$ whereas in (d), (e) and (f) they are parallel to $\langle 110 \rangle$. The heavily shaded arrows show the spin directions on the Mn atoms at height 1/4, and the lightly shaded ones those on atoms at height 3/4.

Domains will be present in magnetic structures which have symmetry lower than that of the paramagnetic phase and the number of different domains will be equal to the order of the symmetry element which is relaxed. More generally, if the symmetry of the paramagnetic group is G and that of the magnetic group M, then there exists a subgroup S such that S × M = G and the number of different domains is given by the order of S. In calculating magnetic diffraction intensities the average over all domains must be taken, and it is due to this averaging that both 100 and 110 reflections are predicted for the (c) and (f) structures above. It is particularly important to take proper account of the different domains when discussing the polarization analysis results.

3. The technique of generalized polarization analysis

Our measurements have been made using the CRYOPAD polarimeter described by Tasset *et al* (1988) and by Tasset (1989). The heart of the device is a liquid helium cryostat fitted with a variable temperature insert in which the specimen temperature may be set in the range 2–300 K. The specimen can be rotated about the vertical axis under the control of a dedicated PDP11/73 computer. The specimen chamber is surrounded by two concentric superconducting Meissner screens between which are two superconducting solenoids with their axes vertical, one fixed to intercept the incident neutron beam and the other, moveable, to intercept the Bragg scattered beam. The screens are cooled below their superconducting transition temperature in a shielded region of zero magnetic field. Outside this cryostat, the incident and scattered neutron beams pass through adiabatic spin-field rotators. On the incident side, the polarized beam from the parent IN20 triple axis spectrometer at the Institut Laue–Langevin, Grenoble first passes down a tubular collimator containing a longitudinal magnetic guide field and then enters a region of transverse field. The angle between this field and the vertical can be set by the computer to any desired nutation angle θ. In the scattered beam the sequence of fields is reversed—first transverse, then longitudinal—before the beam enters the graphite

filter, Mezei spin flipper, Heusler alloy analyser and detector which are all part of the normal IN20 configuration.

The incident beam polarization at the sample position can be set to any desired direction by a suitable combination of nutation angle θ and current in the vertical coil which causes the polarization to precess by an angle Φ while passing between the outer and inner Meissner shields. Similarly, only appropriate choices of Φ and θ in the scattered beam will deliver the full scattered polarization parallel to the horizontal magnetization direction of the analyser. In addition to calculating the setting the rotation angle for the specimen, the CRYOPAD computer can position the output precession coil, set the required values of input and output θ and Φ, instruct IN20 to set the appropriate angles for analyser and detector and then carry out a flexible sequence of measurements at the desired specimen temperature.

A special technique has been developed to determine the scattered polarization corresponding to a given incident polarization (or vice-versa) which proceeds as follows. First the ratio R between the counting rates for flipper on and off is measured for three settings of the output angles: $\Theta_{out} = 90°\ \phi_{out} = 0$, $\Theta_{out} = 90°\ \phi_{out} = 90°$, $\Theta_{out} = 0°$ $\phi_{out} = 0°$. The corresponding polarizations given by $(1 - R)/(1 + R)$ give the components of the scattered polarization P_X, P_Y, P_Z where Y is parallel to the diffracted beam, Z is vertical and X completes a right-handed orthogonal set. These three measurements are used to estimate the precession $\phi_{out} = \phi_m = 180 - \tan^{-1}(P_Y/P_X)$ after which, with $\Theta_{out} = 90°$, the polarization would be positive and maximized. With $\Theta_{out} = 90°$, R is again measured for a few values of ϕ_{out} near to $\phi_m - 90°$. At this position the polarization should be nearly zero and the dependence of P on ϕ_{out} linear with a slope of $\sqrt{(P_X^2 + P_Y^2)}$ radians^{-1}. These data may therefore be used to find the precession $\phi_{out} = \phi_0$ at which $P = 0$ with good precision. With $\phi_{out} = \phi_0 + 90°$ a similar procedure is used to locate the position $\Theta_{out} = \Theta_0$ at which the polarization is again zero using $\Theta_0\ \cos^{-1}(P_Z/\sqrt{(P_X^2 + P_Y^2 + P_Z^2)}) - 90°$ and knowing that the gradient of P with respect to Θ_{out} at this point is $\sqrt{(P_X^2 + P_Y^2 + P_Z^2)}$ radians^{-1}. Finally with $\Theta_{out} = \Theta_0 + 90°$ and $\phi_{out} = \phi_0 + 90°$ measurement of R gives the magnitude of the scattered polarization which has spherical polar coordinates $\Theta = \Theta_0 + 90°$, $\phi = 90° - \phi_0$ with respect to the X, Y, Z axes defined above. It can be shown that with this technique, and assuming instrumental aberrations are negligible, the uncertainty in any one component of the polarization is just the statistical uncertainty in the determination of the polarizations at the zero polarization points. This whole procedure has been programmed for the PDP11 computer, so that given a setting of either the input or output coils, the corresponding scattered or incident polarization can be measured automatically.

4. Experimental measurements

The crystal used in the present experiments was kindly given to us by S Tomiyoshi: it had been quenched from 900 °C and was in the form of a disk cut perpendicular to c approximately 3 mm thick and 5 mm diameter. The susceptibility and spontaneous magnetization of a sample from the same ingot have been measured by Ohmori (1986) and are shown in figure 2. The crystal was mounted with an $\langle 010 \rangle$ axis vertical on the central axis of the CRYOPAD cryostat. At a temperature of 200 K the satellite reflections characteristic of the incommensurate phase were not found, so it was concluded that this phase did not occur in the sample and a series of measurements was made at 200 K. The crystal was set to the peaks of the reflections 100, 10$\bar{1}$, 10 −1 and
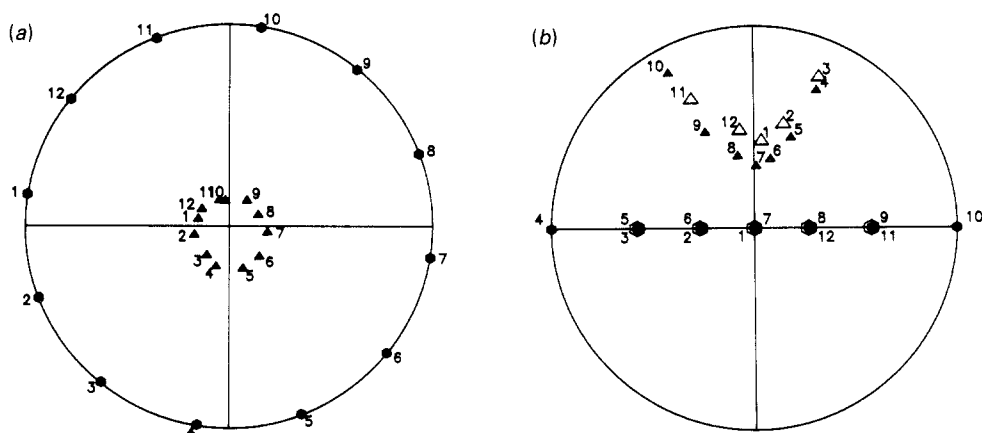
Figure 4. Stereographic projection of the incident and scattered polarization directions for the 100 (*a*) and 101 (*b*) reflections from Mn_3Sn at 200 K. In (*a*) the incident polarization direction is being scanned in the (010) plane whilst in (*b*) it is scanned in the vertical plane containing the 101 scattering vector. The incident directions are marked by hexagons and the scattered directions by triangles, the filled symbols mark poles in the upper and open symbols those in the lower hemisphere. The number to the left of each symbol is the sequence number of the point in the scan and can be used to identify corresponding incident and scattered directions.

102 in turn. For each Bragg peak the direction of the input polarization was scanned, first in the plane perpendicular to the scattering vector (x), then in the vertical plane containing x (y-scan) and finally in the horizontal plane (z-scan). Each scan was over a full 360° in 13 steps of 30° so that the first and last points were identical and gave a check on stability. At each point of the scan the magnitude and direction of the polarization of the diffracted beam were determined using the procedure explained above. The results of these measurements may be displayed by representing the input and output polarizations as points on a stereographic projection. Figure 4(*a*) shows the results of the z-scan of the 100 and 4(*b*) the y-scan of the $10\bar{1}$ reflection in this way. Such figures give a good qualitative appreciation of the rotation of the polarization of the scattered beam with respect to the incident beam, but to obtain quantitative information about the structure it is necessary to consider both the magnitude and direction of the polarization. In this context it is useful to define orthogonal axes x, y, z with x parallel to the scattering vector, z vertical (perpendicular to the incident and diffracted beams) and y completing the right-hand set; these are the axes of the polarization scans described above. The components, with respect to these axes, of both incident and scattered polarizations for selected points of the scans are tabulated in table 1 as a more quantitative record of the results obtained at 200 K.

Another series of measurements was carried out at temperatures below 200 K. it was immediately found that a very significant additional depolarization took place on cooling below about 50 K. This is consistent with an abrupt increase in the ferromagnetic moment to a level at which depolarization in the domain walls becomes important. Figure 5 shows the temperature dependence of polarization scattered parallel to [010] by the 100 reflection for incident polarization also parallel to [010]; it can be seen that between 60 K and 40 K a transition takes place in which all scattered polarization in this direction is lost.

Table 1. Components of incident and diffracted polarization for the 100, 101 and 102 reflections of Mn₃Sn at 200 K. The axes are defined with x parallel to the scattering vector, z vertical and y completing the right-handed set.

Incident polarization			Scattered polarization								
			Reflection 001			Reflection 101			Reflection 102		
P_x	P_y	P_z	P_x	P_y	P_z	P_x	P_y	P_z	P_x	P_y	P_z
0.00	0.00	0.88	−0.02	−0.01	0.78	−0.02	0.32	0.49	0.04	0.38	0.54
0.44	0.00	0.76	0.00	−0.01	0.67	−0.10	0.28	0.44	0.15	0.38	0.43
0.76	0.00	0.44	0.02	0.00	0.42	−0.13	0.33	0.25	0.21	0.37	0.24
0.88	0.00	0.00	0.03	0.00	0.09	−0.14	0.34	0.06	0.22	0.38	0.03
0.76	0.00	−0.44	0.33	0.01	−0.25	−0.13	0.37	−0.13	0.19	0.39	−0.18
0.44	0.00	−0.76	0.04	0.01	−0.06	−0.07	0.40	−0.31	0.11	0.44	−0.40
0.00	0.88	−0.01	0.01	0.03	0.13	−0.01	0.33	−0.07	0.01	0.57	0.06
−0.01	0.76	−0.45	0.00	0.04	−0.22	−0.01	0.35	−0.07	0.01	0.57	−0.09
−0.01	0.43	−0.77	0.02	0.03	−0.57	0.00	0.37	−0.23	0.00	0.56	−0.27
−0.02	−0.01	−0.88	0.02	0.01	−0.75	0.01	0.41	−0.38	−0.02	0.47	−0.45
−0.01	−0.45	−0.76	0.01	0.00	−0.60	0.02	0.42	−0.39	−0.04	0.27	−0.50
−0.01	−0.77	−0.43	0.00	−0.03	−0.26	0.03	0.39	−0.17	−0.05	0.02	−0.24
0.00	−0.88	0.01	−0.01	−0.04	0.10	0.04	0.35	0.14	−0.04	−0.09	0.18
0.01	−0.76	0.45	−0.01	−0.04	0.42	0.01	0.34	0.42	0.01	0.02	0.52
0.01	−0.43	0.77	−0.02	−0.02	0.67	0.00	0.33	0.53	0.03	0.21	0.63
0.02	0.01	0.88	−0.01	0.01	0.78	−0.01	0.33	0.49	0.03	0.39	0.54
0.01	0.45	0.76	−0.04	0.00	0.69	−0.01	0.32	0.36	0.02	0.49	0.37
0.01	0.77	0.43	−0.01	0.03	0.45	0.00	0.32	0.21	0.02	0.54	0.21

To investigate the low temperature magnetic phase further, polarization scans of the 100, 101 and 002 reflections, similar to those made at 200 K, were carried out at 5 K. The results are summarized in table 2 which gives the components of incident and scattered polarization for a selection of points from the scans. The results for the 101 and 100 reflections are very similar and the scattered beam is almost completely
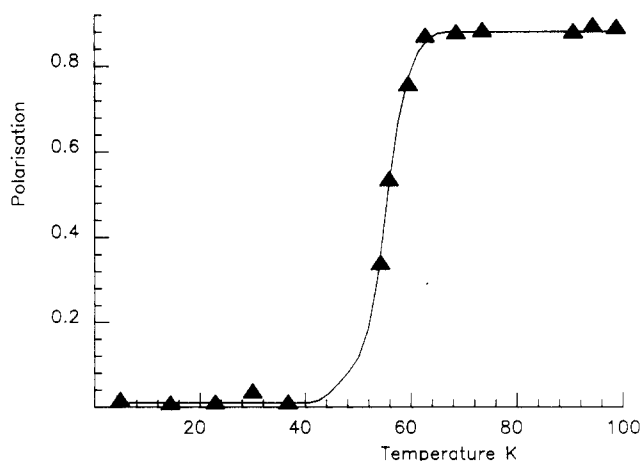
Figure 5. Polarization of the beam scattered by the 100 reflection as a function of temperature. The incident polarization is parallel to [010].

depolarized. For the purely nuclear 002 reflection, however, the components of polarization in the (001) plane are destroyed whilst those parallel to [001] are preserved in all the scans. The components of polarization in table 2 are given on crystallographic axes to make this point clear. Such depolarization could arise from magnetic scattering by randomly populated antiferromagnetic domains if the magnetic scattering were much greater than the nuclear scattering; however, this cannot be the case for the 002 reflection which must have a zero magnetic structure factor for any antiferromagnetic arrangement of manganese spins. It seems more likely that the depolarization of the 002 reflection is due the existence of ferromagnetic domains and their associated domain walls, with the ferromagnetic moment parallel to the direction in which the polarization is preserved namely [001]. If such is the case then the depolarization in the 101 and 100 reflections is due to the combination of that due to ferromagnetic and antiferromagnetic domains. Table 2 shows that what little polarization is scattered by these reflections is, as for the 002 reflection, parallel to [001]. The existence of a large ferromagnetic component of moment along [001] is in agreement with the observations of Ohmori et al (1987) and Tomiyoshi et al (1987) (figure 2) who find an increase in the spontaneous magnetization parallel to [001] below 100 K.

5. Determination of the structure from the scattered polarizations

The relationship between the incident and scattered polarizations P_i and P_o may be expressed by a tensor equation:

$$P_{oj} = \mathbf{A}_{ij}P_{ij} + P_{ci}. \tag{1}$$

In which the first term gives the rotation of the polarization which may be accompanied by a change of amplitude and the second term describes a polarization P_c which is created in the scattering process. The components of $\mathbf{A}$ and P_c can be calculated from the equation given by Blume (1963) as

$$\mathbf{A}_{ij} = [\delta_{ij}(NN^* - Q.Q^*) + 2\mathrm{Re}(Q_iQ_j^*) + 2\mathrm{Im}(\varepsilon_{ijk}(Q_kN^*))]/I \tag{2}$$

$$P_{ci} = 2\mathrm{Re}(Q_iN^*) + 2\mathrm{Im}(\varepsilon_{ijk}(Q_kQ_j^*))/I \tag{3}$$

$$I = NN^* + 2\mathrm{Re}(NP.Q^*) + (Q.Q^*) + i[P.(Q \times Q^*)]$$

where N is the nuclear structure factor and Q the generalized magnetic interaction vector: $\delta_{ij} = 1$ if $i = j$ and is otherwise 0; $\varepsilon_{ijk} = 0$ if any of the three indices are identical and is otherwise $+$ or -1 depending on whether ijk is a cyclic permutation of xyz or not. I is a normalizing factor equal to the total scattered intensity.

It can be seen that only the third term in equation (2) can cause rotation of the polarization out of the Q–P plane and only the second term in equation (3) can create polarization perpendicular to Q. In none of the scans with input polarization in the plane perpendicular to the scattering vector was any significant component of the scattered polarization found to be out of this plane. This observation provides evidence that the magnetic structure factors are real in accordance with current models of the magnetic structure. A qualitative analysis of the scans of the 100 reflection indicates that Q for this reflection is along the vertical [010] direction and that a mixture of domains with oppositely directed Qs leads to the strong depolarization observed when the incident polarization is in the horizontal plane. This provides strong evidence that the moments have no component in the [001] direction: i.e. they lie in the basal plane in contradiction

Table 2. Components of incident and scattered polarization for the 002, 101 and 100 reflections of Mn₃Sn at 5 K with respect to orthogonal crystallographic axes: (100), [010] and [001].

Reflection	(002)			(101)			(100)		
	P_{a^*}	P_b	P_c	P_{a^*}	P_b	P_c	P_{a^*}	P_b	P_c
Input	0.00	0.88	0.01	0.00	0.88	0.00	0.00	0.88	0.00
Output	0.05	0.14	0.05	0.04	0.06	−0.10	−0.02	0.01	0.00
Input	0.01	0.76	0.44	0.30	0.76	0.33	0.52	0.71	0.00
Output	0.05	0.09	0.45	0.01	0.05	−0.16	−0.02	0.01	0.00
Input	0.02	−0.01	0.88	0.53	0.44	0.56	0.84	−0.27	0.00
Output	0.02	−0.05	0.73	−0.02	0.02	−0.19	−0.02	0.01	0.00
Input	0.01	−0.76	0.44	0.60	0.00	0.65	0.52	−0.71	0.00
Output	−0.03	−0.14	0.36	−0.02	0.00	−0.19	−0.02	0.00	0.00
Input	0.01	0.88	0.02	0.52	−0.44	0.56	0.01	0.28	0.83
Output	0.05	0.15	0.03	−0.01	−0.02	−0.17	−0.02	0.00	−0.05
Input	0.45	0.76	0.00	0.30	−0.76	0.32	0.01	0.72	0.51
Output	0.12	0.09	0.03	−0.01	−0.05	−0.13	−0.02	0.01	−0.03
Input	−0.88	0.01	0.02	−0.60	0.01	0.65	0.02	0.88	−0.01
Output	−0.15	0.04	−0.03	−0.02	0.00	−0.08	−0.02	0.01	0.00
Input	−0.43	0.77	0.03	−0.10	0.01	0.87	0.01	0.70	−0.53
Output	−0.05	0.13	0.03	−0.04	0.00	−0.14	−0.02	0.01	0.04
Input	−0.87	0.01	0.16	0.43	0.00	0.77	0.14	0.01	0.87
Output	−0.14	0.02	0.12	−0.03	0.00	−0.18	−0.02	0.01	−0.05
Input	−0.67	0.01	0.57	0.80	−0.01	0.37	0.62	0.01	0.62
Output	−0.11	0.00	0.45	0.00	0.00	−0.18	−0.03	0.00	−0.04
Input	0.16	−0.01	0.87	0.86	−0.01	−0.17	0.87	0.00	0.14
Output	0.05	−0.05	0.72	0.02	0.01	−0.15	−0.02	0.00	−0.01
Input	0.83	−0.01	0.30	0.60	−0.01	−0.65	0.78	−0.01	−0.40
Output	0.14	−0.05	0.23	0.05	0.01	−0.09	−0.02	0.00	0.02

to the original work of Kouvel and Kasper (1968) but in accord with the more recent studies.

A more quantitative analysis requires further development of the equations given above for the particular case of the triangular structures of figure 1. Table 3 lists the magnetic interaction vectors Q for $h0l$-type reflections for the six structures of figure 3. They are given in terms of γ, defined to be one half of the ratio between the magnetic and nuclear structure factors. As in section 4, orthogonal right-handed axes are defined with x parallel to the scattering vector and z vertical, so Q has only y and z components. In each case the Qs for all possible domains are given. Structures (a) and (d) have the full symmetry of the chemical space group, so the only domains are of the 180° type for which the direction of all the spins are reversed and the phase of Q relative to that of the nuclear structure factor changes by 180°. Structures (b) and (e) are those lacking the symmetry planes perpendicular to the $\langle 100 \rangle$ and $\langle 1 - 10 \rangle$ axes, so two domains related

Table 3. Magnetic interaction vectors Q of $h0l$-type reflections for the different magnetic structure models illustrated in figure 1. They are given in units of γ; one half of the ratio of the magnetic to nuclear structure factors. The constant $b = \cos(\tan^{-1}(ha^*/lc^*))$.

Domain	(a)		(b)		(c)		(d)		(e)		(f)	
	Q_y	Q_z	Q_y	Q_z	Q_y	Q_z	Q_y	Q_z	Q_y	Q_z	Q_y	Q_z
1	0	2γ			0	2γ	$2\gamma b$	0			$2\gamma b$	0
2			$\gamma b\sqrt3$	γ	$\gamma b\sqrt3$	γ			γb	$\gamma\sqrt3$	γb	$\gamma\sqrt3$
3			$-\gamma b\sqrt3$	γ	$-\gamma b\sqrt3$	γ			$-\gamma b$	$\gamma\sqrt3$	$-\gamma b$	$\gamma\sqrt3$
4	0	-2γ			0	-2γ	$-2\gamma b$	0			$-2\gamma b$	0
5			$-\gamma b\sqrt3$	$-\gamma$	$-\gamma b\sqrt3$	$-\gamma$			$-\gamma b$	$-\gamma\sqrt3$	$-\gamma b$	$-\gamma\sqrt3$
3			$\gamma b\sqrt3$	$-\gamma$	$\gamma b\sqrt3$	$-\gamma$			γb	$-\gamma\sqrt3$	γb	$-\gamma\sqrt3$

by these symmetry planes are present together with their 180° partners. Structures (c) and (f) have three domains related by the missing triad axis, again each with its 180° partner. The domains have been numbered so as to emphasize the relationship between the Qs for the different structures. Thus Q for domain 1 of structures (c) and (f) is the same as that for structures (a) and (d) respectively and the Qs for the domains (2 and 3) of (b) and (e) are identical to those of domains 2 and 3 of structures (c) and (f). Similar relationships for the general reflections explain why the different structures cannot be distinguished from intensity measurements alone.

In order to get an initial idea of how the scattered polarization depends on both the structure model and the domain populations, it is useful to calculate the scattered components of polarization in the principal directions (x, y, z) for polarization incident in each of these three principal directions in turn. It is convenient to express the domain populations α_n (where α_n is the fraction of the volume of the crystal in which the magnetic structure is that of domain n) in terms of the linear combinations:

$$c_1 = \alpha_1 + \alpha_4 \qquad c_3 = \alpha_2 + \alpha_3 + \alpha_5 + \alpha_6 \qquad c_5 = \alpha_2 - \alpha_3 - \alpha_5 + \alpha_6$$

$$c_2 = \alpha_1 - \alpha_4 \qquad c_4 = \alpha_2 + \alpha_3 - \alpha_5 - \alpha_6 \qquad c_6 = \alpha_2 - \alpha_3 + \alpha_5 - \alpha_6.$$

Defining P_{ij} as the component of scattered polarization parallel to i for incident polarization parallel to j and noting that for some models some of the coefficients α are constrained to be zero, the following relationships can be deduced for models (a), (b) and (c):

$$P_{xx} = 1 - \gamma^2[4c_1 + (3b^2 + 1)c_3]/D_x$$

$$P_{zx} = \gamma(2c_2 + \sqrt{3}c_4)/D_x$$

$$P_{xy} = 0$$

$$P_{zy} = [2\sqrt{3}\gamma^2 bc_6 + \gamma(2c_2 + \sqrt{3}c_4)]/D_y$$

$$P_{xz} = 0$$

$$P_{zz} = [1 + \gamma^2[4c_1 - (3b^2 - 1)c_3] + \gamma(2c_2 + \sqrt{3}c_4)]/D_z$$

$$P_{yx} = 2\sqrt{3}\gamma bc_5/D_x$$

$$D_x = 1 + \gamma^2[4c_1 + (3b^2 + 1)c_3]$$

$$P_{yy} = \{1 - \gamma^2[4c_1 - (3b^2 - 1)c_3] + 2\sqrt{3}\gamma bc_5\}/D_y$$

$$D_y = 1 + \gamma^2[4c_1 + (3b^2 + 1)c_3] + 2\sqrt{3}\gamma bc_5$$

$$P_{yz} = (2\sqrt{3}b\gamma^2 c_6 + 2\sqrt{3}\gamma bc_5)/D_z$$

$$D_z = 1 + \gamma^2[4c_1 + (3b^2 + 1)c_3] + \gamma(2c_2 + \sqrt{3}c_4)$$

where γ is one half of the ratio of the magnetic to nuclear structure factors. D_j is proportional to the total scattered intensity with input polarization parallel to j. The constant $b = \cos(\tan^{-1}(ha^*/1c^*))$.

Similarly, for models (d), (e) and (f):

$$P_{xx} = [1 - \gamma^2\{4b^2c_1 + (b^2 + 3)c_3\}]/D_x$$

$$P_{zx} = 2\sqrt{3}\gamma c_4$$

$$P_{xy} = 0$$

$$P_{zy} = [2\sqrt{3}\gamma^2 bc_6 + 2\sqrt{3}\gamma c_4]/D_y$$

Table 4. Values of the polarizations measured in the three principal directions for the 101 reflection at 200 K.

P_{ij} $\overset{j}{\underset{i}{\diagdown}}$	x	y	z
x	−0.21	0.01	0.00
y	0.43	0.43	0.42
z	0.07	0.09	0.63

Table 5. Values of γ_{101}, the constants c_i and the domain populations α_i deduced from the polarizations in the three principal directions given in table 4. The columns labelled α_i(LSQ) give the results of the least squares analysis using all the measured data. The results for the models with spins parallel to $\langle 100 \rangle$ (model (c)) and $\langle 110 \rangle$ (model (f)) are given respectively in the left- and right-hand parts of the table. The moment per manganese atom is $\gamma_{101} \times 4.18$ in Bohr magnetons.

	Model (c)			Model (f)		
i	c_i	α_i	α_i(LSQ)	c_i	α_i	α_i(LSQ)
1	0.32	0.24	0.191(7)	0.30	0.30	0.331(7)
2	0.15	0.38	0.333(8)	0.30	0.33	0.275(7)
3	0.68	0.06	0.049(4)	0.70	0.06	0.115(4)
4	0.19	0.09	0.144(4)	0.07	0.00	0.00
5	0.57	0.00	0.00	0.46	0.06	0.060(13)
6	0.07	0.25	0.283(12)	0.08	0.25	0.219(6)
γ		0.70	0.718(2)		0.78	0.719(2)

$$P_{xz} = 0$$
$$P_{zz} = [1 - \gamma^2\{4b^2c_1 + (b^2 - 3)c_3\} + 2\sqrt{3}\gamma c_4]/D_z$$
$$P_{yx} = 2\gamma b(2c_2 + c_5)/D_x$$
$$D_x = 1 + \gamma^2[4b^2c_1 + (b^2 + 3)c_3]$$
$$P_{yy} = \{1 + \gamma^2[4b^2c_1 + (b^2 - 3)c_3] + 2\gamma b(2c_2 + c_5)\}/D_y$$
$$D_y = 1 + \gamma^2[4b^2c_1 + (b^2 + 3)c_3] + 2\gamma b(2c_2 + c_5)$$
$$P_{yz} = [2\sqrt{3}b\gamma^2c_6 + 2\gamma b(2c_2 + c_5)]/D_z$$
$$D_z = 1 + \gamma^2[4b_2c_1 + (b^2 + 3)c_3] + 2\sqrt{3}\gamma c_4.$$

These equations can be used to estimate values for γ and the domain populations which can subsequently be used as starting values in a least squares refinement involving all the measured polarizations.

The initial estimate of parameters is based on the observation that the P_{xx} term has the form $(1 - q)/(1 + q)$ which allows q and hence D_x to be determined. The estimation of γ and the constants c is then straightforward. For the $h0l$ reflections the constants c_2 and c_4 always occur in the combination $2c_2 + \sqrt{3}c_4$ for the (c) structure and hence cannot be determined independently: the same type of relationship exists between c_2 and c_5 for structure (f). The measurements of the 101 reflection in the principal directions are given
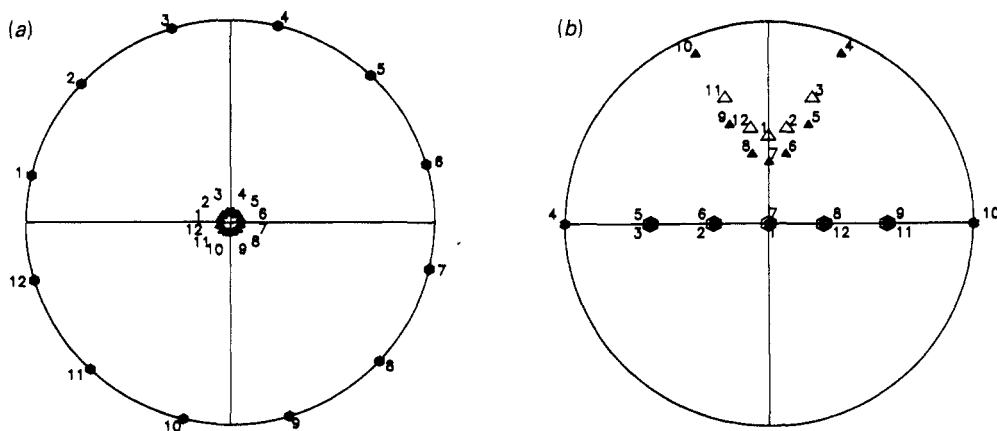
Figure 6. Stereographic projections of the directions of polarization scattered by the 100 (*a*) and 101 (*b*) reflections predicted from the refined structure model for incident polarization directions as in figure 4. The poles are marked in the same way as in figure 4.

in table 4 and values of the parameters for the two cases which have been estimated from them in table 5. Domain populations α_i consistent with these values, subject to the constraints that $0 \leq \alpha \leq 1$ for all the αs and that the sum of all αs must be unity are also shown in table 5. It should be noticed that for both sets of models the constants c_1 and c_3 are significantly different from zero indicating that only a three domain model, i.e. the 'inverse triangle' structures (*c*) and (*f*) will fit the data. The final columns of table 5 give the domain populations and the value of γ which have been refined from these values by making a least squares fit to the polarization scans of the 100, 10$\bar{1}$, 10 -1 and 102 reflections. As pointed out, above the αs are not all independently determined by the data so only four αs are refined in each case: the fifth is given an arbitrary fixed value and the sixth determined by the normalization condition. The choice of which of the αs to fix is nearly but not completely arbitrary: for instance setting c_2 to zero ($\alpha_1 = \alpha_4$) in model (*f*) leads to negative values for α_3, α_5 and α_6. In fact the high value of P_{yx} in table 4 suggests a large imbalance between domains 1 and 4 and therefore α_4 has been set to zero for model (*f*). Similar considerations suggest that the population of domain 5 for model (*c*) must be small and it has been fixed as zero. Fixing the smallest domain populations as zero avoids spurious values emerging from the least squares refinement.

The final values of γ and the domain parameters are listed in table 5 and the goodness of fit χ^2 calculated using the estimated values for the standard deviations of the components of polarization was 3.5 for both models (*c*) and (*f*). Figure 6 gives the stereographic projections of the incident and scattered polarization directions calculated from the model which are directly comparable with observed projections of figure 4.

6. Discussion

There is essentially no difference in the goodness of fit between the observed and calculated polarizations for models (*c*) and (*f*). The reason for this is that, although there is significant imbalance in the populations of equivalent 180° domains, the division of the crystal amongst the three trigonal domains is very nearly equal. It can be shown that in the case of exact equality no difference in the scattered polarizations would be predicted. The magnetic moment obtained in both cases is 3.00(1) μ_B, very much larger

than the value $1.78\,\mu_B$ obtained by Tomiyoshi (1982) from his polarized neutron measurements on a magnetized sample.

A recent calculation by Sticht *et al* (1989) based on a local approximation to spin-density functional theory suggests that the magnetic moment on Mn should be $\simeq 3\,\mu_B$, in agreement with the value we find.

The final χ^2 is quite satisfctory, but suggests that some instrumental aberrations still remain so that the precision of the scattered polarization directions is overestimated. However, even at this level of development it is clear that the technique of generalized polarization analysis is capable of measuring the ratio of magnetic to nuclear scattering with an accuracy of around 0.5%. This level of accuracy is as good, if not better than that obtainable with the classical polarized neutron method, in cases where the ratio of magnetic to nuclear scattering is large. The technique has the added advantage that the amplitude of magnetic scattering is determined essentially independently of the domain populations.

The present experiment indicates unequivocally that the magnetic structure of Mn_3Sn is one allowing at least three domains and the results are completely compatible with the inverse triangle structure. The question of the easy magnetization direction in zero field and hence of the true magnetic space group remains unresolved, but it is possible that a unique answer could be obtained by using the present technique on a previously magnetized sample for which the trigonal domains should be unequally populated.

Acknowledgments

References

Blume M 1963 *Phys. Rev.* **130** 1670
Kádár G and Krén E 1971 *Int. J. Magn.* **1** 143
Kouvel J S and Kasper J S 1965 *Proc. Conf. on Magnetism (Nottingham, 1964)* (London: Institute of Physics) p 169
Krén E and Kádár G 1970 *Solid State Commun.* **8** 1653
Nagamiya T, Tomiyoshi S and Yamaguchi Y 1982 *Solid State Commun.* **42** 385
Ohmori H, Tomiyoshi S, Yamaguchi H and Yamamoto H 1987 *J. Magn. Magn. Mater.* **70** 249
Ohmori H 1986 *MSc Thesis* Tohoku University (in Japanese)
Ohoyama T 1961 *J. Phys. Soc. Japan* **16** 1995
Sticht J, Höck K-H and Kübler J 1989 *J. Phys.: Condens. Matter* **1** 8155
Tasset F 1989 *Physica B* **156–157** 627
Tasset F, Brown P J and Forsyth J B 1988 *J. Appl. Phys.* **63** 3606
Tomiyoshi S 1982 *J. Phys. Soc. Japan* **51** 803
Tomiyoshi S, Abe S, Yamaguchi Y, Yamaguchi H and Yamamoto H 1986 *J. Magn. Magn. Mater.* **54–57** 1001
Tomiyoshi S and Yamaguchi Y 1982 *J. Phys. Soc. Japan* **51** 2478
Tomiyoshi S, Yoshida H, Ohmori H, Kaneko T and Yamamoto H 1987 *J. Magn. Magn. Mater.* **70** 247
Yasukochi K, Kanematsu K and Ohoyama T 1961 *J. Phys. Soc. Japan* **16** 1123
Zimmer G J and Krén E 1972 *Magnetism and Magnetic Materials 1971 (AIP Conf. Proc. No 5)* (New York: American Institute of Physics) p 513
——— 1973 *Magnetism and Magnetic Materials 1972 (AIP Conf. Proc. No 10)* (New York: American Institute of Phys) p 1379